Dobslaw, H., Flechtner, F., Bergmann-Wolf, I., Dahle, C., Dill, R., Esselborn, S., Sasgen, I., Thomas, M. (2013): Simulating high-frequency atmosphere-ocean mass variability for de-aliasing of satellite gravity observations: AOD1B RL05. - Journal of Geophysical Research, 118, 7, 3704-3711

DOI: 10.1002/jgrc.20271

JOURNAL OF GEOPHYSICAL RESEARCH, VOL. ???, XXXX, DOI:10.1029/,

Simulating High-Frequency Atmosphere-Ocean Mass Variability for De-Aliasing of Satellite Gravity Observations: AOD1B RL05

H. Dobslaw[1], F. Flechtner[1], I. Bergmann-Wolf[1], Ch. Dahle[1], R. Dill[1], S. Esselborn[1], I. Sasgen[1], M. Thomas[1]

Henryk Dobslaw, Deutsches GeoForschungsZentrum (GFZ), Dep. 1: Geodesy and Remote Sensing, Potsdam, Germany. (dobslaw@gfz-potsdam.de)

[1]Deutsches GeoForschungsZentrum GFZ,
Department 1: Geodesy and Remote
Sensing, Potsdam, Germany.

Abstract. An improved version of the OMCT ocean model with 1° spatial resolution provides bottom pressure anomalies for the new release 05 of the GRACE Atmosphere and Ocean De-aliasing Level 1B (AOD1B) product. For high-frequency signals with periods below 30 days, this model explains up to 10 cm^2 of the residual sea level variance seen by ENVISAT in large parts of the Southern Ocean, corresponding to about 40% of the observed sea level residuals in many open ocean regions away from the tropics. Comparable amounts of variance are also explained by AOD1B RL05 for co-located in situ ocean bottom pressure recorders. Although secular trends contained in AOD1B RL05 cause GRACE KBRR residuals to increase in shallow water regions, we find a reduction of those residuals over all open ocean areas, indicating that AOD1B RL05 is much better suited to remove non-tidal high-frequency mass variability from satellite gravity observations than previous versions of AOD1B.

1. Introduction

For about one decade now, time-variations in the Earth's gravity field have been monitored by the Gravity Recovery and Climate Experiment [GRACE; *Tapley et al.*, 2004] satellite mission. This novel data-set provides valuable insight into a number of mass redistribution phenomena on Earth that include ice-mass changes and their relation to global atmospheric circulation patterns [*Sasgen et al.*, 2010] and contribution to sea level [*Jacob et al.*, 2012], terrestrial water storage variations and groundwater depletion [*Rodell et al.*, 2009], co-seismic displacements associated with major earth-quakes [*Han et al.*, 2006], ocean tides in ice-covered seas [*Mayer-Gürr et al.*, 2012], or large-scale ocean bottom pressure variations and their relation to the time-varying winds [*Boening et al.*, 2011].

The Earth's gravity field is precisely measured by satellite-to-satellite tracking of one pair of spacecrafts trailing each other in a non-repeat polar orbit at currently 440 km altitude. While one revolution is completed in roughly 90 minutes, data from typically 30 days are accumulated to calculate a global gravity field model. The deviations of those approximately monthly gravity fields - the monthly mean GRACE gravity field solutions - from their long-term mean can be subsequently related to geophysical processes in the solid Earth and its fluid envelope.

However, tides and, to a lesser extent, also non-tidal variations in atmospheric pressure, wind induced ocean currents, and terrestrial water storage changes associated with major precipitation events cause detectable gravitational signals on sub-monthly time-scales. Not accounting for such short-term variations that are not resolvable by the monthly GRACE sampling causes aliasing artifacts in the monthly mean solutions, and therefore reduces the accuracy of those gravity field models in particular at smaller spatial scales. In order to make use of the full potential of satellite gravimetry measurements, high-frequency signals need to be either removed from the observations by means of background models, or properly taken into account within the parameter estimation process.

Although recent experiments show promising results for the latter approach [*Kurtenbach et al.*, 2009], non-tidal variability is typically corrected for by using the time-variable background model GRACE Atmosphere and Ocean De-aliasing Level 1B Product [AOD1B; *Flechtner*, 2007], that is based on pressure, temperature, and moisture fields from 6-hourly operational atmospheric analyses of the European Centre for Medium Range Weather Forecasts (ECMWF), and ocean bottom pressure grids from the Ocean Model for Circulation and Tides [OMCT; *Thomas et al.*, 2001].

Besides being used for de-aliasing purposes in the GRACE processing since 2006, release 04 (RL04) of AOD1B and its underlying OMCT simulation has been applied in a number of studies in other branches of geodesy that include the interpretation of Earth rotation variations [e.g., *Dobslaw et al.*, 2010], or terrestrial gravity observations from superconducting gravimeters [*Kroner et al.*, 2009]. However, several weaknesses of AOD1B RL04 have been identified [e.g., *Bonin and Chambers*, 2011, see also the summary at www.gfz-potsdam.de/AOD1B], during the years. Consequently, a new release 05 (RL05) of AOD1B has been calculated, dedicated to an improved de-aliasing of non-tidal ocean mass variability in the GRACE gravity field processing.

In this contribution, the characteristics of the OMCT ocean model configuration used to calculate AOD1B RL05 are described. The high-frequency component of the simulated ocean bottom pressure is validated against sea level variability from satellite altimetry and sparsely distributed in situ ocean bottom pressure gauges. The new AOD1B version is subsequently tested for its ability to reduce the residuals of the k-band range-rate (KBRR) measurements between the two GRACE spacecrafts, which serves as an indicator for the reduction of aliasing artifacts in the monthly mean GRACE gravity field solutions. Finally, simulated secular trends in AOD1B will be presented and discussed with respect to their potential leakage into regional surface mass balance estimates of the major ice-sheets.

2. OMCT Configuration for AOD1B RL05

While the atmospheric part of the AOD1B remains unchanged in the new release, the OMCT model version applied for AOD1B RL05 is an evolution of an earlier model configuration described by *Dobslaw and Thomas* [2007]. It is discretized on a 1° latitude-longitude grid, with 20 layers in the vertical. The time-step has been reduced to 20 min in order to comply with stability criterions. As before, OMCT is forced with atmospheric surface pressure, surface wind stresses, 2m-temperatures, and atmospheric freshwater fluxes provided every 6 hours by the ECMWF operational analyses. Fluctuations in total ocean mass due to the incorporation of the Boussinesq approximation in OMCT and imbalances in applied freshwater fluxes are adjusted at each time-step by means of a globally homogeneous shell of mass added to the top layer of the model. No river runoff has been considered in OMCT simulations used for any AOD1B version. Also, dynamic feedbacks due to loading and self-attraction effects of the water column [e.g. *Kuhlmann et al.*, 2011] are not considered in AOD1B RL05.

By means of several sensitivity experiments, horizontal eddy viscosity and vertical momentum transfer parameters were adjusted to align the simulated bottom pressure and sea level variability with available observations. The simulation finally chosen for AOD1B

RL05 is based on an initial spin-up run with climatological atmospheric boundary forcing, followed by real-time simulations with ERA Interim forcing (1989-2000) and subsequently operational ECMWF forcing since Jan 1st, 2001, both with a temporal resolution of 6 hours. The time-mean circulation is generally consistent with a previous OMCT run discussed in detail by *Dobslaw* [2007].

As for earlier AOD1B versions, OMCT is forced by 6-hourly atmospheric fields that contain sub-diurnal variability related to atmospheric tides, which cause secondary oceanic tides due to periodic atmospheric pressure loading and wind stresses [*Dobslaw and Thomas*, 2005]. Whereas diurnal signals are retained in AOD1B, we remove the (partially aliased) semi-diurnal variability from the bottom pressure grids by means of a correction model obtained from a harmonic fit over the years 2001-2002, since ocean bottom pressure variability at this frequency is already contained in the ocean tide background models applied separately in the GRACE processing. Atmospheric tides are, however, variable in time, leading to small residual tidal signals with a period of 12 hours in AOD1B. Regularly updated estimates on those residual tidal signals are available at the web-page www.gfz-potsdam.de/AOD1B. Further technical details about those new simulations contained in AOD1B RL05 are provided within an updated version of the official AOD1B document [*Flechtner and Dobslaw*, 2013], which is available at the GRACE archives.

Although AOD1B contains ocean bottom pressure variability with respect to a mean field over the period 2001-2002 at all frequencies, we primarily focus in the remainder of this paper on high-frequency variability with periods shorter than 30 days, since correcting for those signals is the primary goal of the AOD1B background model. In the new release 05 (Fig. 1), strongest variability at those scales is found in the Southern Pacific and also in mid-latitudes of the North Pacific and the Nordic Seas. Almost no bottom pressure variability is predicted by the model around the equator: wind-driven bottom pressure signals are generally tiny in tropical latitudes, whereas changes in total ocean mass that might be observed here [*Hughes et al.*, 2012] are excluded from OMCT simulations for AOD1B as discussed above.

The (publicly available) AOD1B product contains four different sets of Stokes coefficients characterising the disturbing potential caused by anomalous masses in atmosphere and ocean. 'Atm' describes the contribution of the vertically distributed atmospheric masses, 'ocn' the contribution of the water column as simulated by OMCT, 'glo' the combined effect of 'atm' and 'ocn', whereas 'oba' represents the bottom pressure simulated by OMCT that is forced by atmospheric surface pressure and other meteorologic quantities from the lower boundary of the atmosphere. Thus the difference between 'oba' and 'glo' is meant to reflect only effects of vertically shifted atmospheric masses, which are generally assumed to be very small. The monthly mean averages of those products typically delivered with the GRACE gravity field solutions are labelled GAA, GAB, GAC and GAD, respectively. In the remainder of this study, we use 'oba' coefficients and its underlying gridded pressure anomalies for the validation against OBP and sea level, whereas 'glo' coefficients are used for the KBRR residual analysis.

3. Validation Against In Situ Ocean Bottom Pressure and ENVISAT Sea Level Anomalies

To validate the high-frequency variability content in AOD1B RL05 over the oceans, we utilize both in situ ocean bottom pressure (OBP) gauges and sea level anomalies from satellite altimetry. Globally distributed OBP datasets collected by various institutions were made available by *Macrander et al.* [2010]. The provided data are checked for outliers, instrumental drifts are removed by a quadratic fit, and tidal signals are eliminated with the FES2004 ocean tide model [*Lyard et al.*, 2006] and a subsequently applied Doodson filter [*IOC*, 1985]. As a second data-set, we use sea level anomalies from satellite altimetry [ENVISAT RA2 GDR v2.1; *ESA*, 2011] over the period 2003 - 2008 as a proxy for short-term ocean mass variations as suggested by *Bonin and Chambers* [2011].

Along-track ellipsoidal sea surface heights are corrected for the recommended instrumental and geophysical effects as provided within the Geophysical Data Records, including a radiometer-based correction for the influence of the wet troposphere and an inverse barometer correction. Ionospheric travel-time delays are corrected using GIM [*Schaer*, 1999], sea state bias is accounted for by following the approach of *Gaspar et al.* [1994], ocean tides and ocean loading are taken from GOT4.7 [*Ray*, 1999]. After optionally applying an additional correction model for ocean bottom pressure-related sea level anomalies based on AOD1B RL04 or RL05, along-track sea level residuals are finally interpolated daywise onto 1° latitude-longitude grids using search radii of 300 km.

In order to focus on high-frequency variability, a 3rd order Butterworth filter with 30 days cutoff period is applied to all time-series. Globally gridded sea-surface height anomalies at those periods (Fig. 2; no AOD1B-based correction model applied) are dominated by meso-scale variability adjacent to western boundary currents, which represents density anomalies in upper-ocean waters that are not reflected in bottom pressure variability. In mid-latitudes and away from the western boundaries, wind and pressure variations driven by synoptic weather patterns cause sea-surface height anomalies of a few cm that are essentially barotropic and therefore equally present in co-located OBP gauges, whose high-pass filtered variability has been overlaid to Fig. 2 by means of color-coded triangles.

Based on those residual sea level and bottom pressure anomalies, we attempt to test the ability of AOD1B to further reduce the variability of both independent observational data-sets. We therefore convert the 6-hourly simulated bottom pressure anomalies from AOD1B into equivalent sea-water heights by using a mean sea-water density of 1028 kg m^{-3} and apply them as an additional geophysical correction model to the along-track ENVISAT observations. Equally, simulated bottom pressure is subtracted from the in situ OBP observations. The variances in sea-level and bottom pressure that are explained by AOD1B are subsequently interpreted as a measure of model skill in predicting short-term ocean mass anomalies.

For RL04, we find absolute explained variances of about 10 cm^2 in different parts of the Southern Pacific, the South China Sea, the Gulf of Carpentaria and in the central North Pacific. In large regions of the South Atlantic and Indian Ocean, however, explained variances are actually negative (Fig. 3, upper left), suggesting that the model has no skill in predicting ocean mass variability in those areas. Variances in sea level explained by the new release (Fig. 3, upper right) instead approach 10 cm^2 in effectively all parts of the Southern Ocean that are not dominated by meso-scale variability. In addition, AOD1B RL05 explains in the Nordic Seas up to 50% of residual sea level variance (Fig. 3, lower right), which indicates a substantial skill of the model given that upper-ocean processes not related to mass redistribution are still contained in the ENVISAT observations. RL05 has, however, deficiencies in the Gulf of Carpentaria, where more variance in sea level is explained by the older model version compared to RL05. Apparently, Torres Strait between Australia and New Guinea is too deep and too wide in the model bathymetry used for AOD1B RL05, thereby prohibiting the realistic simulation of the free oscillations in that semi-enclosed region.

We also evaluated sea level anomalies from Jason-1 over the same time-span and found generally consistent results (not shown). An exception is the strong sea level variability seen by ENVISAT off the Chilean coast at 40°S, 100°W. This feature is neither explained by AOD1B RL04 or RL05, nor has it been captured by Jason 1, suggesting that it is due to observation or processing errors in the ENVISAT satellite altimetry data-set used here.

Variances explained by AOD1B RL04 and RL05 in observations of (30 day high-pass filtered) in situ OBP residuals are expressed in cm^2 of equivalent water height and overlaid to Fig. 3 by means of color-coded triangles. Absolute values of variances explained for individual gauges are locally very consistent with the results obtained for ENVISAT, indicating that both independent observation groups are equally well explained by the AOD1B model data. Relative explained variances are, however, substantially higher for the OBP observations than for ENVISAT. This applies in particular to the lower latitudes, where bottom pressure signals are small and sea-level variability is dominated by upper ocean baroclinicity. Whereas RL04 typically only explains a few percent of the observed bottom pressure variance, we find positive relative explained variances for almost all OBP records under consideration, many of them approaching or even exceeding 50%.

4. Impact on GRACE KBRR Residuals

We further evaluate the skill of both AOD1B versions in reducing the residuals of the k-Band range-rates measured between the two GRACE spacecrafts, here for the year 2008. Those residuals are obtained from the standard GRACE gravity field processing at

GFZ, where all background models and processing standards are fixed to RL05 standards [*Dahle et al.*, 2012], and only the AOD1B model has been replaced by the old AOD1B RL04 version.

Blockmean averages on a 2° latitude-longitude grid are calculated for KBRR residuals after applying AOD1B RL04 and RL05. Differences (Fig. 4, left) indicate that the remaining residuals are generally lower for RL05 over most of the Southern Ocean, suggesting that RL05 is indeed able to better explain range-rate anomalies between the two spacecrafts that are caused by gravitational effects of time-variable oceanic masses. However, in several regions increasing KBRR residuals are identified when changing from RL04 to RL05, as, e.g., near the Patagonian and the Siberian Shelf, or in Hudson Bay.

In order to separate the impact of high-frequency variability from signals at seasonal periods and longer, we derive two series of sub-monthly AOD1B products by calculating and subsequently removing monthly mean fields. By doing so, only the variability at periods below 30 days is retained, similar to high-pass filtering the sea level variability and in situ OBP in the previous section. For those sub-monthly AOD1B products (Fig. 4, right), KBRR residuals are consistently smaller when applying RL05 instead of RL04, supporting our conclusion that RL05 better explains non-tidal ocean mass variability than the previous AOD1B version.

5. Trends Simulated in OMCT

OMCT simulations are intended to simulate in particular short-term variability in ocean bottom pressure in response to rapidly varying atmospheric conditions. In the long run, however, the model is drifting more rapidly than, e.g., current state-of-the-art coupled climate models that are prepared to reproduce climate variability over many centuries. Low frequency variability and trends in OMCT ocean bottom pressure (Fig. 5) are primarily related to ongoing warming and cooling of water masses at intermediate depths, and its secondary effects on the thermohaline circulation. They are therefore much less reliable than the high-frequency variability and should not be interpreted geophysically.

The AOD1B coefficients are applied as an a priori time-variable background model in the gravity field estimation process. Thus, any trends included in AOD1B are expected to be reflected additive-inversely in the monthly GRACE gravity fields, the so-called GSM products. To assess their potential impact on estimating secular trends from GRACE over the major ice-sheets, we apply the inversion method by *Sasgen et al.* [2010] to estimate spatial leakage of oceanic signals towards the continents. We estimate regional averages for both the major drainage basins of Antarctica as defined in Fig. 1 of *Sasgen et al.* [2012a], as well as of the Greenland ice-sheet as defined in Fig. 1 of *Sasgen et al.* [2012b]. In addition to the original AOD1B trends, we also invert AOD1B trend estimates filtered in the spatial domain by an isotropic Gaussian average filter of 4° width, to arrive at conservative estimates for the potential influence of the oceanic leakage.

For Greenland (Tab. 1), negative ocean bottom pressure trends of about 0.5 hPa a^{-1} in AOD1B RL05 cause artifical positive mass trends over the northern parts of Greenland (mainly basins A and B) of up to 2.1 Gt a^{-1}, thus decreasing ice-mass losses over those regions obtainable from the GRACE GSM products by this amount. Simulated positive ocean bottom pressure trends in Hudson Bay instead contribute to more negative mass trends in western Greenland (basins F and G) of up to -2.3 Gt a^{-1} as seen by the GSM fields. For the whole ice-sheet, however, positive and negative contributions compensate each other, leading to a weakly negative effect of the AOD1B RL05 trends to the mass balance of Greenland as represented by the GRACE GSM products.

For the Antarctic ice-sheet (Tab. 2), positive trends in AOD1B RL05 in the Ross Sea and also around the Antarctic Peninsula lead to artificial negative mass trends of up to -2.6 Gt a^{-1} (basins 19, 24, and 25). Positive bottom pressure trends instead are found in the Amundsen Sea Sector (basin 20), and in various parts of East Antarctica. When averaged over the whole continent, however, we note an overall negative mass trend of -11.7 Gt a^{-1}. Based on those numbers, we judge the potential impact of oceanic leakage on secular trend estimates to be small, but non-negligible, although we are aware that the amount of leakage may vary depending on the GRACE filtering and inversion scheme applied. It is therefore advisable to restore the monthly mean of the applied AOD1B products over the oceans (i.e. the GAD products) to the GSM monthly mean gravity fields, before estimating long-term mass changes in the vicinity of oceanic regions.

6. Summary and Outlook

A revised version of the OMCT ocean model [*Thomas et al.*, 2001] discretized on a 1° latitude-longitude grid has been forced with 6-hourly ECMWF operational analysis fields to simulate time-series of ocean bottom pressure since 2001 with high temporal resolution and typical latencies of five days. The water column part of the simulated bottom pressure has been combined with vertically distributed masses in the atmosphere as represented by the ECMWF analyses to form a new release 05 of the GRACE Atmosphere and Ocean De-aliasing Level 1B Product [AOD1B; *Flechtner*, 2007].

The quality of the new AOD1B has been validated for periods shorter than 30 days, since accurate reproduction of mass variability not resolveable by the nominal GRACE sampling of 30 days is particularly important to avoid aliasing artifacts in the GRACE gravity field solutions. RL05 explains variances of high-pass filtered residual sea level anomalies from ENVISAT by about 10 cm^2 in large parts of the Southern Ocean that are not dominated by meso-scale eddies, meaning that RL05 is able to explain about 40% of the residual sea level variability. Since also upper-ocean processes as well as observation and processing errors contribute to the sea level residuals discussed here, we conclude that the dynamical processes leading to sub-monthly mass redistributions in the oceans are well represented in the latest version of AOD1B. This conclusion is also supported by an analysis of in situ ocean bottom pressure gauges, which shows generally comparable amounts of variance explained by AOD1B in most regions.

By testing the ability of the new AOD1B for reducing GRACE KBRR residuals, we find substantial improvements over the previous AOD1B version in most open ocean areas away from the tropics. Increasing residuals in shallow water regions are attributed to secular trends that are more pronounced in RL05 than in RL04. Those trends are primarily related to ongoing adjustment processes of the thermohaline circulation as represented in OMCT, and are therefore assumed to be largely artifical.

Since high-frequency mass variations in the oceans affect a broad range of geodetic and geophysical observation types, the new AOD1B model time-series might be well suited for applications outside the GRACE project, as, e.g., the interpretation of changes in the Earth's rotation or station deformations due to non-tidal atmospheric and oceanic loading. The value of AOD1B for such efforts has been already formally acknowledged by the International Earth Rotation and Reference Systems Service (IERS) by assigning AOD1B the status of an official product of its Global Geophysical Fluid Center (GGFC) in

May 2012. In addition, the series might be used to separate the primarily wind-driven sea level variations from steric height contributions seen by satellite altimetry before assessing the regional oceanic heat budget, as it is currently already beeing done at AVISO for Jason 1 with numerical model data from the global barotropic ocean model MOG2D-G [*Carrère and Lyard*, 2003] and its more recent sucessors.

For a homogeneous re-processing of the GRACE mission period, however, the latest AOD1B version still has deficits as, e.g., the (presumably artificial) trends in the oceanic part of AOD1B, or sudden shifts in atmospheric masses over mountainous regions that are related to changes in the horizontal and vertical discretization of the ECMWF model [*Duan et al.*, 2012]. Future work will both be focussing on the homogeniety of the time-series as well as on the reproduction of signals with smaller spatial scales. This will be in particular important since the satellite laser link to be flown as a demonstrator on the GRACE-FO mission after 2017 is expected to increase the sensitivity of that new mission by up to two orders of magnitude [*Sheard et al.*, 2012], which makes aliasing of short-term and small-scale variability a potentially limiting factor for the overall mission accuracy.

Acknowledgments. We thank Deutscher Wetterdienst, Offenbach, Germany, and the European Centre for Medium-Range Weather Forecasts, Reading, U.K., for providing data from ECMWF's operational forecast model. OMCT simulations were performed at Deutsches Klimarechenzentrum, Hamburg, Germany. The European Space Agency is acknowledged for providing ENVISAT radar altimeter data. This work has been supported by Deutsche Forschungsgemeinschaft within the priority program SPP1257 "Mass Transport and Mass Distribution in the System Earth" under grant DO1311/2-1.

References

Boening, C., T. Lee, and V. Zlotnicki (2011), A record-high ocean bottom pressure in the South Pacific observed by GRACE, *Geophys. Res. Lett.*, *38*, L04602.

Bonin, J. A., and D. P. Chambers (2011), Evaluation of high-frequency oceanographic signal in GRACE data: Implications for de-aliasing, *Geophys. Res. Lett.*, *38*, L17608.

Carrère, L., and F. Lyard (2003), Modeling the barotropic response of the global ocean to atmospheric wind and pressure forcing - comparisons with observations, *Geophys. Res. Lett.*, *30*(6), 1997–2000.

Dahle, C., F. Flechtner, C. Gruber, D. Koenig, R. Koenig, G. Michalak, and K.-H. Neumeyer (2012), GFZ GRACE Level-2 Processing Standards Document for Level-2 Product Release 0005, *Tech. rep.*, GeoForschungsZentrum.

Dobslaw, H. (2007), Modellierung der allgemeinen ozeanischen Dynamik zur Korrektur und Interpretation von Satellitendaten, *Tech. rep.*, Scientific Technical Report 07/10, Deutsches GeoForschungsZentrum, Potsdam, Germany.

Dobslaw, H., and M. Thomas (2005), Atmospheric induced oceanic tides from ECMWF forecasts, *Geophys. Res. Lett.*, *32*(10), L10615.

Dobslaw, H., and M. Thomas (2007), Simulation and observation of global ocean mass anomalies, *J. Geophys. Res.*, *112*(C05), C05040.

Dobslaw, H., R. Dill, A. Grötzsch, A. Brzeziski, and M. Thomas (2010), Seasonal polar motion excitation from numerical models of atmosphere, ocean, and continental hydrosphere, *J. Geophys. Res.*, *115*, B10406.

Duan, J., C. K. Shum, J. Guo, and Z. Huang (2012), Uncovered spurious jumps in the GRACE atmospheric de-aliasing data: potential contamination of GRACE observed mass change, *Geophys. J. Int.*, *2*, 1–5.

ESA (2011), ENVISAT Altimetry Level 2 User Manual v1.4.

Flechtner, F. (2007), GRACE AOD1B Product Description Document for Product Releases 01 to 04, *Tech. rep.*, Rev. 3.1, GRACE Document 327-750, GeoForschungsZentrum Potsdam, Potsdam, Germany.

Flechtner, F., and H. Dobslaw (2013), GRACE AOD1B Product Description Document for Product Release 05, *Tech. rep.*, Rev. 4.0, GRACE Document 327-750, GeoForschungsZentrum Potsdam, Potsdam, Germany.

Gaspar, P., F. Ogor, P.-Y. Le Traon, and O.-Z. Zanife (1994), Estimating the sea state bias of the TOPEX and POSEIDON altimeters from crossover differences, *J. Geophys. Res.*, *99*(C12), 24981–24994.

Han, S., C. Shum, M. Bevis, C. Ji, and C. Kuo (2006), Crustal dilatation observed by GRACE after the 2004 Sumatra-Andaman earthquake, *Science*, *313*, 658–662.

Hughes, C. W., M. E. Tamisiea, R. J. Bingham, and J. Williams (2012), Weighing the ocean: Using a single mooring to measure changes in the mass of the ocean, *Geophys. Res. Lett.*, *39*(17), L17602.

IOC (1985), Manual on Sea Level Measurement and Interpretation - Volume 1: Basic Procedures, *IOC Manual and Guides*, *14*.

Jacob, T., J. Wahr, W. T. Pfeffer, and S. Swenson (2012), Recent contributions of glaciers and ice caps to sea level rise., *Nature*, *482*, 514–518.

Kroner, C., M. Thomas, H. Dobslaw, M. Abe, and A. Weise (2009), Seasonal effects of non-tidal oceanic mass shifts in observations with superconducting gravimeters, *J. Geod.*, *48*, 354–359.

Kuhlmann, J., H. Dobslaw, and M. Thomas (2011), Improved modeling of sea level patterns by incorporating self-attraction and loading, *J. Geophys. Res.*, *116*(C11), C11036.

Kurtenbach, E., T. Mayer-Gürr, and A. Eicker (2009), Deriving daily snapshots of the Earth's gravity field from GRACE L1B data using Kalman filtering, *Geophys. Res. Lett.*, *36*, L17102.

Lyard, F., F. Lefevre, T. Letellier, and O. Francis (2006), Modelling the global ocean tides: modern insights from FES2004, *Ocean Dynamics*, *56*(5), 394–415.

Macrander, A., C. Boening, O. Boebel, and J. Schroeter (2010), Validation of GRACE gravity fields by in-situ data of ocean bottom pressure, in *System Earth via Geodetic-Geophysical Space Techniques*, edited by F. Flechtner, pp. 169–185, Springer, Berlin.

Mayer-Gürr, T., R. Savcenko, W. Bosch, I. Daras, F. Flechtner, and C. Dahle (2012), Ocean tides from satellite altimetry and GRACE, *J. Geod.*, *59-60*, 28–38.

Ray, R. (1999), *A global ocean tide model from TOPEX/Poseidon altimetry: GOT99.2*, 58 pp., NASA Tech. Memo. 209478, Goddard Space Flight Center, Greenbelt.

Rodell, M., I. Velicogna, and J. S. Famiglietti (2009), Satellite-based estimates of groundwater depletion in India., *Nature*, *460*, 999–1002.

Sasgen, I., H. Dobslaw, Z. Martinec, and M. Thomas (2010), Satellite gravimetry observation of Antarctic snow accumulation related to ENSO, *Earth and Planetary Science Letters*, *299*(3-4), 352–358.

Sasgen, I., H. Konrad, E. R. Ivins, M. R. van den Broeke, J. L. Bamber, Z. Martinec, and V. Klemann (2012a), Antarctic ice-mass balance 2002 to 2011: regional re-analysis of GRACE satellite gravimetry measurements with improved estimate of glacial-isostatic adjustment, *The Cryosphere Discussions*, *6*(5), 3703–3732.

Sasgen, I., M. van den Broeke, J. L. Bamber, E. Rignot, L. S. Sø rensen, B. Wouters, Z. Martinec, I. Velicogna, and S. B. Simonsen (2012b), Timing and origin of recent regional ice-mass loss in Greenland, *Earth and Planetary Science Letters*, *333-334*.

Schaer, S. (1999), Mapping and predicting the Earth's ionosphere using the global positioning system, Ph.D. thesis, University of Berne, Berne, Switzerland.

Sheard, B. S., G. Heinzel, K. Danzmann, D. a. Shaddock, W. M. Klipstein, and W. M. Folkner (2012), Intersatellite laser ranging instrument for the GRACE follow-on mission, *J. Geodesy*, *86*(12), 1083–1095.

Tapley, B. D., S. Bettadpur, J. C. Ries, P. F. Thompson, and M. M. Watkins (2004), GRACE measurements of mass variability in the Earth system., *Science*, *305*, 503–505.

Thomas, M., J. Sündermann, and E. Maier-Reimer (2001), Consideration of ocean tides in an OGCM and impacts on subseasonal to decadal polar motion excitation, *Geophys. Res. Lett.*, *28*(12), 2457–2460.

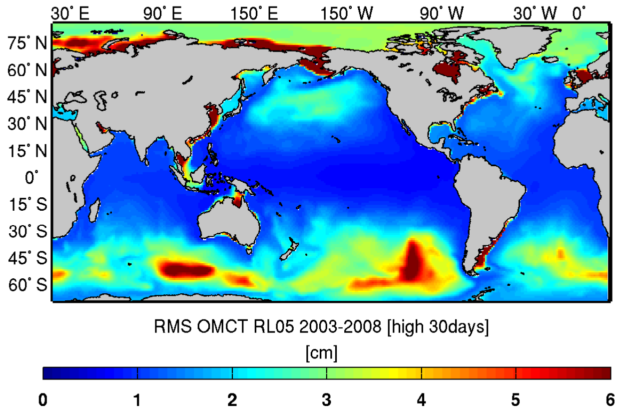

Figure 1. Standard deviation of high-pass filtered (30 days cut-off period) ocean bottom pressure variability simulated with OMCT for AOD1B RL05 (2003 - 2008) which has been expressed in equivalent sea-water height.

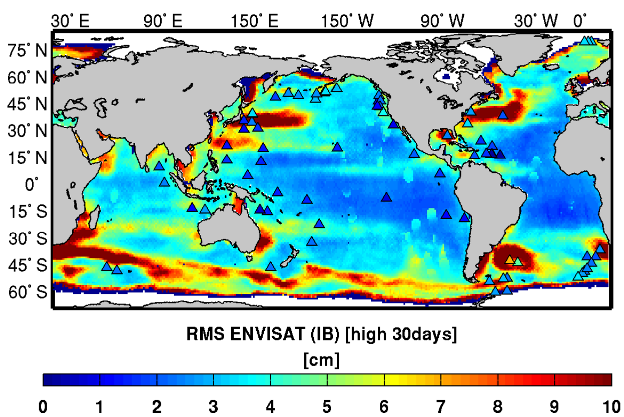

Figure 2. Standard deviation of high-pass filtered (30 days cut-off period) sea level variability from inverse-barometrically corrected ENVISAT observations (2003-2008; gridded at 1° latitude-longitude grid), and ocean bottom pressure variability from ocean bottom pressure (OBP) gauges at sparsely distributed locations (triangles), which has been expressed in equivalent sea-water height.

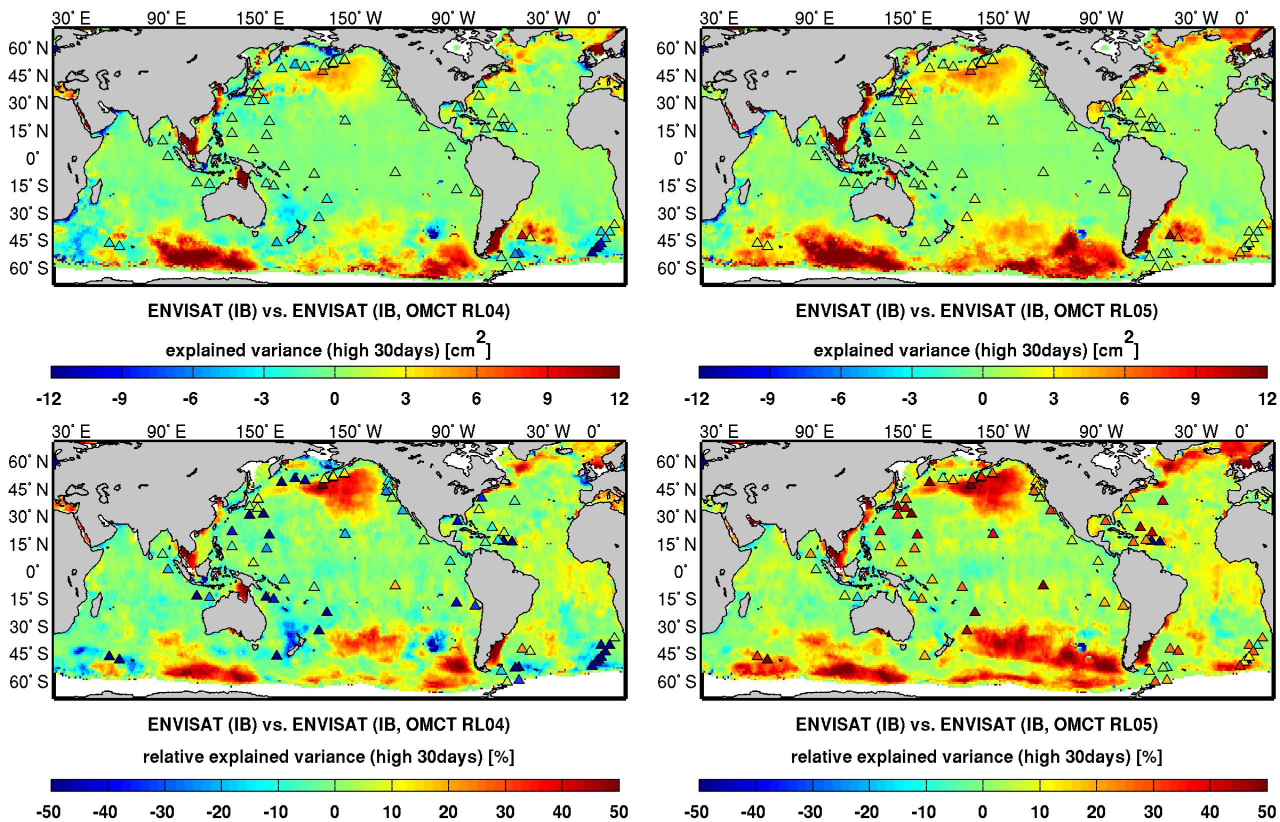

Figure 3. Absolute (top row) and relative (bottom row) variance explained of high-pass filtered (30 days cut-off period) sea level variability from inverse-barometrically corrected ENVISAT observations and in situ OBP gauges expressed in equivalent sea-water heights (triangles) by ocean bottom pressure anomalies taken from AOD1B RL04 (left) and RL05 (right).

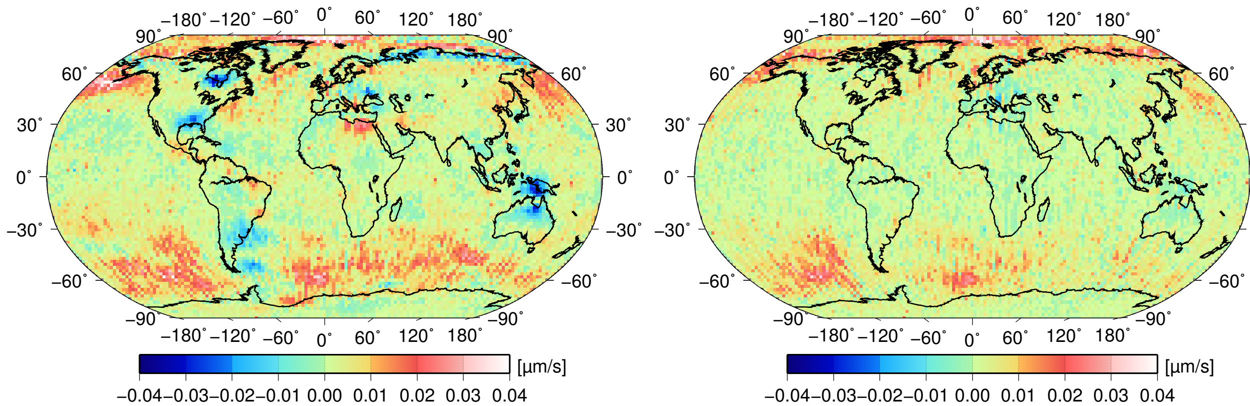

Figure 4. Blockmean averages (2° regular grid) of mean GRACE KBRR residual differences in 2008 after replacing AOD1B RL04 with RL05 (left), and after replacing alternative versions of AOD1B RL04_sm with RL05_sm that have been reduced by their corresponding monthly mean values in order to allow for the evaluation of the high-frequency information content of the AOD1B products only (so-called sub-monthly AOD's, right).

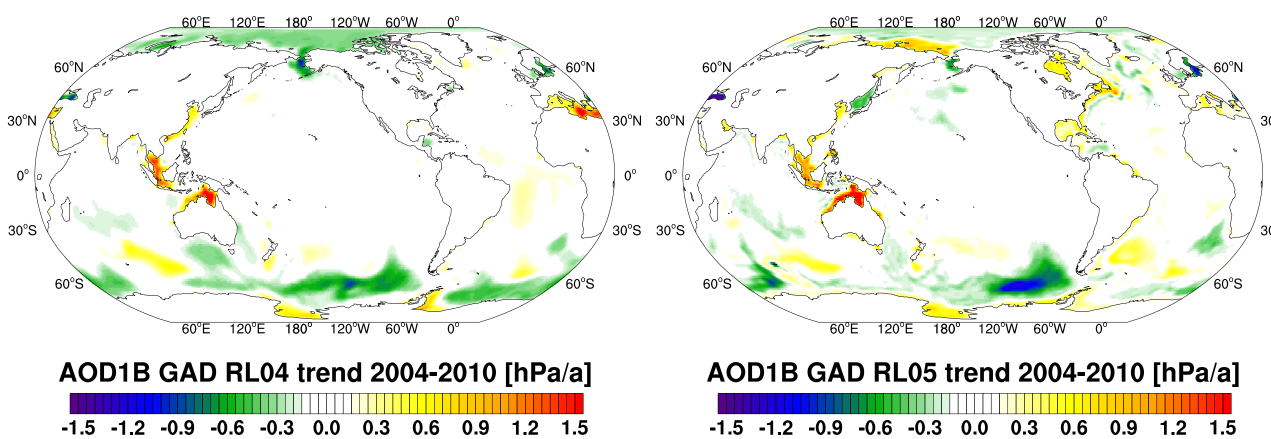

Figure 5. Secular trends in ocean bottom pressure for the period 2004 - 2010 as present in AOD1B RL04 (left) and RL05 (right).

Table 1. Impact of simulated trends in AOD1B RL04 and RL05 on GRACE-based mass-change estimates for individual drainage basins of the Greenland Ice-Sheet as defined by Fig. 1 of *Sasgen et al.* [2012b], both from AOD1B coefficients that are spatially unsmoothed and that are filtered with a 4° isotropic Gaussian filter.

Drainage basin	Area (10^3 km^2)	AOD1B RL04 unfiltered (Gt a^{-1})	AOD1B RL04 filtered (Gt a^{-1})	AOD1B RL05 unfiltered (Gt a^{-1})	AOD1B RL05 filtered (Gt a^{-1})
A	208	1.6	0.6	0.5	1.5
B	439	2.0	3.8	0.7	2.1
C	217	0.9	0.9	0.4	1.0
D	135	0.5	-0.2	-0.1	0.7
E	58	0.9	2.7	0.1	0.2
F	417	1.2	1.9	-0.2	-1.4
G	267	1.1	-0.4	-0.4	-2.3
total	1741	8.2	9.4	1.1	1.8

Table 2. Impact of simulated trends in AOD1B RL04 and RL05 on GRACE-based mass-change estimates for individual drainage basins of the Antarctic Ice-Sheet as defined by Fig. 1 of *Sasgen et al.* [2012a], both from AOD1B coefficients that are spatially unsmoothed and that are filtered with a 4° isotropic Gaussian filter.

Drainage basin	Area (10^3 km^2)	AOD1B RL04 unfiltered (Gt a^{-1})	AOD1B RL04 filtered (Gt a^{-1})	AOD1B RL05 unfiltered (Gt a^{-1})	AOD1B RL05 filtered (Gt a^{-1})
24	369	-1.7	-3.8	-1.0	-2.3
25	104	-1.4	-1.2	-1.3	-1.8
1	342	-0.9	-1.9	-0.3	-0.3
18	414	-0.3	1.3	-0.3	1.2
19	391	-0.1	-2.3	-0.3	-2.6
20	195	0.4	2.8	-0.1	1.9
21	235	0.1	-1.1	-0.04	-0.7
22	175	0.1	1.7	0.3	-0.1
23	96	-0.1	0.2	-0.6	1.1
2	738	-0.3	0.3	-0.2	-0.2
3	1582	-0.3	-2.2	-0.4	-0.5
4	226	0.7	1.7	-0.5	-1.2
5	361	2.4	4.9	-0.2	0.4
6	443	1.6	2.1	0.2	0.4
7	412	1.7	2.2	0.4	0.7
8	243	1.3	3.4	-0.03	0.5
9	963	0.1	-0.03	0.1	0.4
10	335	-0.1	-1.3	-0.2	-0.7
11	690	-0.02	-0.4	-1.0	-2.0
12	1170	0.7	1.6	-0.7	-0.8
13	741	0.5	1.5	-0.7	-0.2
14	147	-0.4	-0.3	-0.7	-1.1
15	281	-0.5	-2.2	-0.8	-1.8
16	1138	-0.4	0.7	-0.6	0.4
17	506	-0.9	-2.5	-0.9	-2.2
total	12297	2.1	5.3	-9.5	-11.7